Int. J. Electrochem. Sci., 17 **(2022)** Article Number: 221032, doi: 10.20964/2022.10.25

International Journal of
ELECTROCHEMICAL
SCIENCE
www.electrochemsci.org

Application of Cu_2O@f-MWCNTs Modified Glassy Carbon Electrode for Electrochemical Detection of Rohypnol as Strong Sedatives and Muscle Relaxers

Xiaochao Yuan[1,*], *Wenhui Su*[2]

[1] AnYang Vocational and Technical College, Anyang 455000, China
[2] College of Chemistry and Environmental Engineering, Anyang Institute of Technology, Anyang 455000, China
[*]E-mail: yxc0372@sina.com, swh@ayit.edu.cn

Received: 7 July 2022 / *Accepted:* 4 August 2022 / *Published:* 10 September 2022

In the current investigation, the glassy carbon electrode has been modified utilizing a nanocomposite of Cu_2O nanoparticles and functionalized (Cu_2O@f-MWCNTs/GCE) by electrodeposition method as a sensitive and selective electrochemical sensor for the measurement of rohypnol (RHP) in human blood plasma. According to SEM and XRD investigations, Cu_2O nanoparticles were randomly arranged on the surface of the f-MWCNTs. This resulted in a high specific surface area and porous architecture, showing that the Cu_2O@f-MWCNTs nanocomposite was successfully electrodeposited on the GCE. The electrochemical studies demonstrated the synergistic effects of the f-MWCNTs with Cu_2O nanoparticles in catalytic reactions for determining RHP. They showed that the incorporation of Cu_2O nanoparticles into the f-MWCNTs enhanced the electrical conductivity pathway within the electrocatalyst reactions and enhanced the electron transfer efficiency at electrode/electrolyte interfaces. The Cu_2O@f-MWCNTs/GCE demonstrated excellent selectivity and sensitivity (0.1769 μA/μM), an acceptable detection limit (15 nM), and a broad linearity range (1 to 160 μM) to determine RHP, which were promoted as superior to or similar to current reports of RHP electrochemical sensors. In order to determine RHP in prepared real samples of human blood plasma, the accuracy and validity of Cu_2O@f-MWCNTs/GCE were assessed. The results showed acceptable recovery (99.40 % to 99.60 %) and low values of RSD (3.22% to 4.87 %), indicating that the developed method has been used successfully to determine RHP in biological liquids.

Keywords: Electrodeposition; Nanocomposite; Cu_2O nanoparticles; Functionalized MWCNTs; Rohypnol; Human blood plasma; amperometry

1. INTRODUCTION

Flunitrazepam, often known as Rohypnol (RHP), is a medication that depresses the central nervous system and lowers the heart rate and respiration rate [1, 2]. The neurotransmitter GABA is

impacted by RHP (gamma amino butyric acid). This can cause severe respiratory depression if the person takes a high dose or combines it with other depressants [3, 4]. It is an intermediate-acting benzodiazepine used to treat severe insomnia and help with anesthesia. Its general features are similar to those of Valium. RHP has sedative-hypnotic, anti-anxiety, and muscle-relaxing properties like other benzodiazepines [5, 6]. As a result, it is used to cure sleeplessness temporarily, as a pre-medication before surgery, and to induce anesthesia. RHP's sedative effects, however, are roughly 7–10 times as potent as Valium [7]. Rohypnol's effects start to take effect 15 to 20 minutes after administration and remain for four to six hours [8, 9]. Certain aftereffects may still be present 12 hours after administration. It can lead to difficulty controlling muscles, forgetfulness, loss of inhibitions, and loss of consciousness in large doses [10].

Rohypnol has been used illegally since the 1990s to treat sadness brought on by the usage of stimulants like cocaine and methamphetamine [11, 12]. RHP is often taken orally, frequently in combination with alcohol. RHP use results in a number of negative effects, including drowsiness, sleepiness, loss of motor control, slowed reaction time, impaired judgment, lack of coordination, slurred speech, aggression or excitability, amnesia (the inability to recall events that occurred while under the influence), stomach disturbances, and respiratory depression with higher doses [13, 14].

Due to RHP's efficacy, it is crucial to determine RHP in clinical and pharmaceutical samples [15, 16]. Numerous studies have been done to improve the sensing performance using gas chromatography-mass spectrometry [17], liquid chromatography atmospheric pressure chemical ionization mass spectrometry [18], fluorescence spectroscopy [19], UV-Vis spectrophotometry [20], desorption electrospray ionization [21], fluorimetry [22] and electrochemical sensors [23-28]. However, the presence of interference chemicals in biological, clinical, and pharmacological samples reduces the accuracy and restricts the use of many of these techniques [29, 30]. Among these sensing techniques, electrochemical approaches have demonstrated sufficient accuracy and selectivity for RHP determination in pharmaceutical, clinical, and biological materials [31, 32]. They are also quick, easy, and inexpensive. More research is needed, according to studies, to improve the detecting capabilities of electrochemical sensors. By modifying the electrode surface with nanostructures, composites, and nanohybrid materials, electrochemical sensors' selectivity and sensitivity can be improved [33-35]. The goal of the current study is to create a nanocomposite of Cu_2O@f-MWCNTs/GCE via electrodeposition that may be used as a sensitive and specific electrochemical sensor to measure RHP, which is a potent sedative and muscle relaxant, in human blood plasma.

2. EXPERIMENT

2.1. Preparation Cu_2O based nanocomposite modified electrode

Electrodeposition method was used for preparation the Cu_2O based nanocomposite modified electrode GCE [36]. First, 0.75 mg of MWCNTs was preserved with 50mL of 6M H_2SO_4/HNO_3 (Sigma-Aldrich) mixtures in the ratio of 1:3 by volume per volume. This suspension was ultrasonically vibrated in a water bath ultrasonic (Branson SFX 550, Shanghai, China) at a temperature of 45 °C for 5

hours. Next, the functionalized MWCNTs (f-MWCNTs) were collected via the discard method and then rinsed thoroughly with deionized water until they reached the neutral pH~7 value of suspension. After then, f-MWCNTs were dehydrated into oven at 70°C for 8 hours. Before the electrodeposition, the GCE surface was polished successively with γ-Al_2O_3 powder (99.99%, 0.1 μm, Sigma-Aldrich) for 12 minutes on polishing cloth (Micropolish II, Buehler, USA), and then washed by ultrasonication with a mixture of water and ethanol for 12 minutes. For preparation of the electrodeposition electrolyte, 200 mg of f-MWCNTs were ultrasonically dispersed in 100 ml of 0.85 M Cu_2SO_4 (≥99.99%, Sigma-Aldrich) and 20 ml of 0.55 M H_2SO_4 solution. Then, the obtained suspension was stirred for 20 minutes. Electrodeposition of Cu_2O@f-MWCNTs on GCE was carried out using an electrochemical workstation potentiostat (CS1005, Zhengzhou CY Scientific Instrument Co., Ltd., China) in three-electrode electrochemical cell setup which contained Ag/AgCl as reference, platinum foil as counter, and GCE as working electrode at potential window from -0.6 V to 0.5 for 40 cycles at a scan rate of 20mV/s. For electrodeposition pure f-MWCNTs on GCE, the procedure was accomplished using an electrolyte without Cu_2SO_4, and for electrodeposition of pure Cu_2O on GCE, the procedure was carried out in electrolyte without f-MWCNTs.

2.2. Instruments

Electrochemical studies have been conducted using differential pulse voltammetry (DPV) and amperometry analyses in an electrochemical workstation potentiostat galvanostat (Xian Yima Optoelec Co., Ltd. China) equipped with a three-electrode electrochemical Pt plate, a cell containing Ag/AgCl and nanostructure modified GCE as counter, reference and working electrodes, respectively. Electrochemical studies were performed into 0.1M PBS electrolyte (pH 7.4) which contained 0.1M NaH_2PO_4 (99%, Sigma-Aldrich) and 0.1M Na_2HPO_4 in an equal volume ratio. A Bruker D8 127 diffraction analyzer (operating at 30 kV and 30 mA, D8 advanced, USA) was used to obtain X-ray diffraction (XRD) patterns of samples. The morphological studies of prepared nanostructures were performed using scanning electron microscopy (SEM; HILIPS XL30/TMP, the Netherlands).

3.2. Study the actual sample from human blood plasma

Cu_2O@f-MWCNTs/suitability GCE's for determining RHP in prepared genuine samples of human blood plasma donated by healthy volunteers was assessed. The samples of human blood plasma were centrifuged at 1000 rpm for 15 minutes, and the supernatant that was produced was filtered and utilized to make 0.1 M PBS (pH 7.4). Then, genuine samples were analyzed using the Human Flunitrazepam ELISA kit and amperometric studies at 0.62 V, and analytical investigations were conducted using the standard addition procedure.

3. RESULTS AND DISCUSSION

3.1. SEM and XRD studies

Figure 1 shows the SEM micrographs of the electrodeposited f-MWCNTs and Cu_2O@f-MWCNTs on GCE. Figure 1a's SEM micrograph of f-MWCNTs demonstrates their spaghetti-like shape and randomly arranged orientation. MWCNTs have a 90 nm diameter on average. The f-MWCNTs and Cu_2O nanoparticles electrodeposited on the electrode surface are visible in the SEM image of the Cu_2O@f-MWCNTs nanocomposite modified GCE. Cu_2O nanoparticles and f-MWCNTs form a powerful covalent link, enhancing the interfacial bonding and reducing agglomeration or bonding between the f-MWCNTs [37, 38]. Moreover, the Cu_2O nanoparticles are randomly decorated on the f-MWCNTs surface, appearing as white spots, which are clearly observed to form white crystal structures of Cu_2O nanoparticles with small sizes and irregular shapes, which create high specific surface area and porous structures.

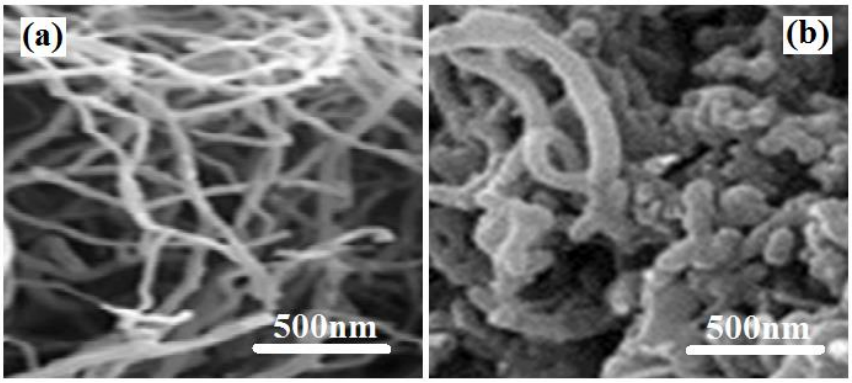

Figure 1. SEMs of electrodeposited (a) f-MWCNTs, (b) Cu_2O@f-MWCNTs on GCE

Figure 2 displays the findings of the structural characterization of powders of electrodeposited f-MWCNTs, Cu_2O, and Cu_2O@f-MWCNT nanocomposite. According to the XRD pattern of the f-MWCNTs, which corresponds to the (002) and (100) reflection of the graphite carbon plane alignment and regularity of the f-MWCNTs (JCPDS card No. 15-1621) [39, 40], functionalization was successful in removing impurities and amorphous carbon without compromising the MWCNTs' structural integrity [41-43]. It is observed from the XRD pattern of Cu_2O, there are diffraction peak at 36.32°, 42.28°, 61.34° and 73.40° which are assigned to (111), (200), (220) and (311) crystalline planes with high crystalline quality of the cubic crystal structure of Cu_2O, respectively (JCPDS card No. 78-2076) [44, 45]. The XRD pattern of the Cu_2O@f-MWCNTs nanocomposite shows both the diffraction peak of the f-MWCNTs and Cu_2O, indicating the successful electrodeposition of well-crystalline Cu_2O@f-MWCNTs nanocomposite on GCE.

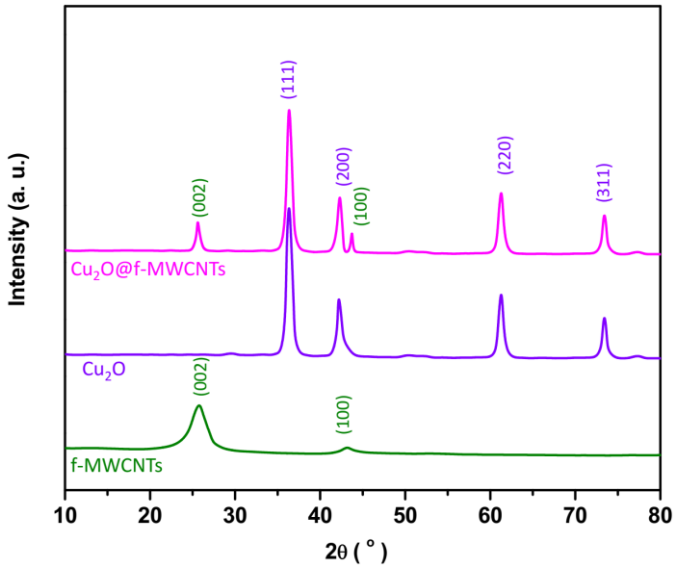

Figure 2. XRD patterns of powders of electrodeposited f-MWCNTs, Cu_2O and Cu_2O@f-MWCNTs nanocomposites

3.2. Electrochemical studies

Figure 3 depicts the CV response of the Cu_2O@f-MWCNTs/GCE in the potential window of -0.90 V to 0.90 V with a scanning rate of 25 mV/s in 0.1 M NaOH as an alkaline environment, which was employed to probe the Cu_2O@f-MWCNTs/electrocatalytic GCE's activities. In accordance with the reports of Dai et al. [46] for Cu2O- bovine serum albumin core-shell nanoparticles modified GCE and Lu et al. [47]. for Cu_2O crystal, it is shown that there are five peaks (A to E), signaling to valence variations of Cu ions. Peak A is ascribed to the oxidation of Cu(0) to Cu at a potential of 0.17 V. (I). Peak B is connected to the oxidation of Cu(I) to Cu at a potential of 0.02 V. (II) [48]. Peak C is connected to the adsorption of OH and the synthesis of soluble compounds from Cu_2O-based solids at a potential of 0.54 V. Peak D at 0.80 V indicates that Cu(III) was formed in a high concentration of NaOH alkaline solution and that Cu(III) was reduced to Cu (II). Peak E at -0.46 V is connected to the conversion of Cu(II) to Cu (I). Therefore, no conversion of Cu(I) to Cu(0) has been seen, indicating that no Cu(0) has been formed during the cycle [46]. These findings support the presence of Cu_2O on the f-MWCNTs/GCE surface and are consistent with XRD findings based on the production of the Cu2O phase on the electrode surface.

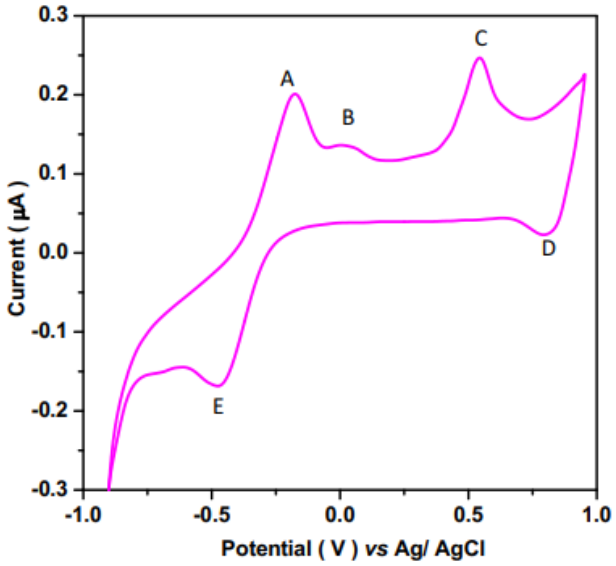

Figure 3. CV response of Cu_2O@f-MWCNTs/GCE at the potential window from -0.90 V to 0.90 V with a scanning rate of 25mV/s in 0.1 M NaOH

Figure 4 shows the DPV curves of the following materials: bare GCE, f-MWCNTs/GCE, Cu_2O/GCE, and Cu_2O@f-MWCNTs/GCE in the potential window of 0.0V to 0.85 V with a scanning rate of 25mV/s into 0.1M PBS in both the absence and addition of 40 M RHP. It is noted that all electrodes fail to exhibit a defining peak in the DPV curves when RHP is absent. Bare GCE's DPV curve does not show a peak in the presence of 100 M RHP, whereas f-MWCNTs/GCE, Cu_2O/GCE, and Cu_2O@f-MWCNTs/GCE show anodic peaks at 0.48 V, 0.44 V, and 0.43 V, respectively, which are associated with RHP oxidation according to the postulated process shown in Figure 5 [26, 49]. The DPV curves show that the peak current of Cu_2O@f-MWCNTs/GCE displays an extremely high peak current at a lower potential of 0.43 V that is approximately 1.3-fold, and 2-fold higher than the peak currents of f-MWCNTs/GCE and Cu_2O/GCE, respectively. Because of the presence of nanopores and the large specific surface area of MWCNTs, the Cu_2O nanoparticles modified electrode exhibits a decrease in oxidation potential toward the f-MWCNTs/GCE [50, 51], and f-MWCNTs exhibit an increase in electrocatalytic current. The functional groups or charged sites of the functionalized molecules serve as the effective active sites for the assembly and anchoring of metal precursors and metal oxide nanoparticles and thereby promote their utilization and electrocatalytic activity [52, 53]. Moreover, the nanoporous network of f-MWCNTs with great electrical conductivity facilitates the charge transfer in electrocatalytic reactions as well as easy accessibility of the reagent molecules to the catalytic sites [52, 54]. Anchoring Cu_2O nanoparticles also shows the high specific surface area and high conductivity provide good electrocatalytic activity and can enhance electron transfer reactions at lower overpotentials [55, 56]. The incorporation of Cu_2O nanoparticles into the f-MWCNTs enhanced the electrical conductivity pathway inside the electrocatalyst reactions and enhanced the electron transfer efficiency at electrode/electrolyte interfaces. Due to the synergistic effects of f-MWCNTs and Cu_2O nanoparticles in catalytic reactions for RHP determination, only Cu_2O@f-MWCNTs/GCE was used in the subsequent electrochemical studies.

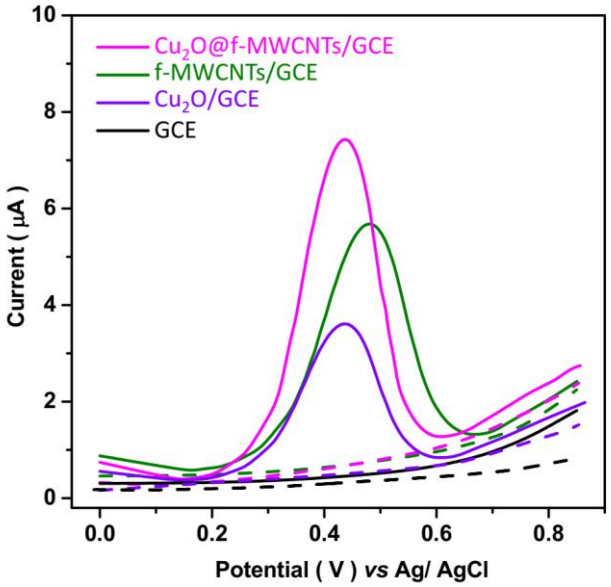

Figure 4. The DPV curves of bare GCE, f-MWCNTs/GCE, Cu_2O/GCE and Cu_2O@f-MWCNTs/GCE at the potential window from 0.0V to 0.85 V with a scanning rate of 25 mV/s in 0.1 M PBS (pH 7.4) in absence (dashed line) and presence (solid line) of 40 μM RHP.

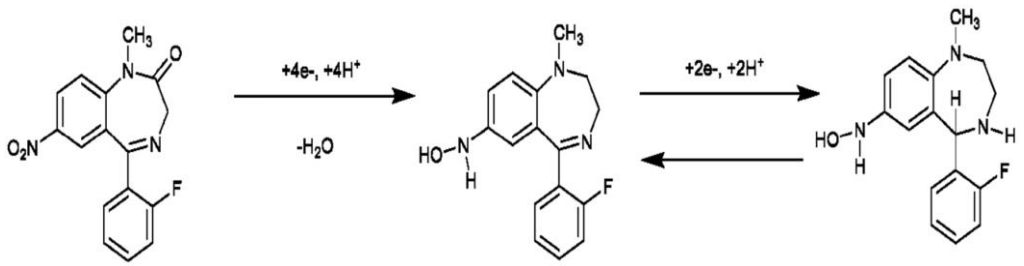

Figure 5. Schematic image of oxidation process of Rohypnol.

Figure 6 shows the amperometry analyses and calibration plot of Cu_2O@f-MWCNTs/GCE after successive injections of 10 M RHP solution into 0.1M PBS (pH 7.4) at a potential of 0.43 V. When RHP is added to the electrolyte solution, the electrocatalytic response is very fast Amperometric response of Cu_2O@f-MWCNTs/GCE increases linearly with each injection of 10 μM RHP solution in the range of 1 to 160 μM. The linear relationship between the electrocatalytic peak current (y) and the RHP concentration (x) is found with a correlation coefficient of 0.99983 as follows [57, 58]:

$$y\ (\mu A) = 0.1769\ x\ (\mu A/\mu M) + 0.0955 \qquad (1)$$

The calibration plot exhibits a sensitivity 0.1769μA/μM, and a detection-limit of 15 nM (S/N=3). Analytical figures of merit for determination of RHP are compared with some reported RHP sensors and the results are tabulated in Table 1. It is observed that the linear range and detection limit of developed RHP sensor in the present study are promoted and are better or comparable with recent reports.

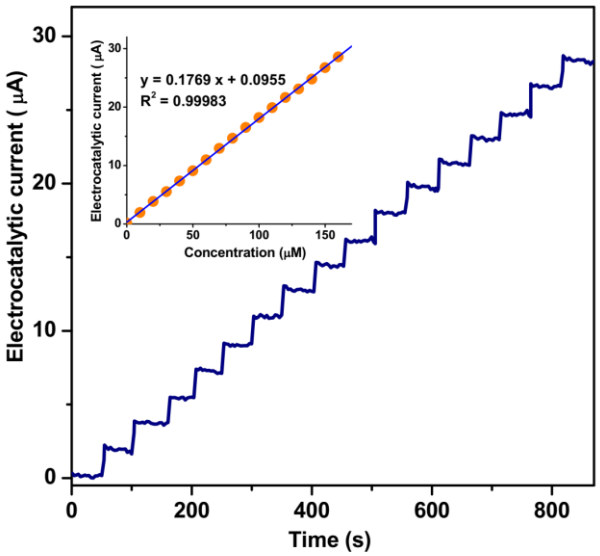

Figure 6. Amperometry analyses and related calibration plot of Cu_2O@f-MWCNTs/GCE after successive injection 10 µM RHP solution into 0.1 M PBS (pH 7.4) at potential of 0.43 V.

Table 1. Analytical figures of merit of some RHP sensors.

Electrode	**Technique**	**LOD (nM)**	**Linear range (µM)**	**Ref.**
Cu_2O@f-MWCNTs/GCE	Amperomertry	15	1 to 160	Present study
Au NPs/$MnFe_2O_4$ NPs/carbon paste electrode	DPV	330	0.1 to 100	[23]
Poly (L-Cystine)/TiO_2@CuO-N-rGO/GCE	DPV	0.3	0.001 to 50	[24]
glucose oxidase/glucose hydrogel droplets/iron-sparked screen printed electrode	DPV	15	1 to 10	[25]
Cu NPs/amine-functionalized graphene oxide/screen printed carbon electrode	DPV	130	0.4 to 140	[28]
Screen printed graphite electrode	CV	19.15	0.032 to 0.64	[26]
Screen printed graphite electrode	CV	1500	3.19 to 30.40	[27]

CV: cyclic voltammetry

In order to study the interference effect on the determination of RHP in human blood plasma samples, the interferences of some substances that exist in biological liquids were investigated using amperomertic tests via Cu_2O@f-MWCNTs/GCE as the working electrode at 0.43 V into 0.1M PBS in addition to 2 µM RHP and 10 µM of interfering substances. The resultant electrocatalytic current is presented in Table 2 which indicates that there is no obvious change in the RHP electrocatalytic current when the interfering compounds are added to the electrolyte solution. Thus, it can be concluded that the proposed RHP sensor exhibits great selectivity for RHP determination in biological liquids.

Table 2. Results of electrocatalytic currents of Cu_2O@f-MWCNTs/GCE using amperomertic analysis at 0.43 *V* into 0.1M PBS in addition 2 µM RHP and 10 µM of interfering substances.

Substance	**Added(µM)**	**Amperomertic current(µA)**	**RSD**
RHP	2	0.3539	±0.0186
l-Cystine	10	0.0722	±0.0041
l-tryptophan	10	0.0611	±0.0021
l-tyrosine	10	0.0623	±0.0034
Glucose	10	0.0380	±0.0012
Dopamine	10	0.0351	±0.0015
Ascorbic acid	10	0.0332	±0.0014
Folic acid	10	0.0721	±0.0020
Uric acid	10	0.0744	±0.0015
Citric acid	10	0.0312	±0.0016
Urea	10	0.0625	±0.0020
Tartaric acid	10	0.0702	±0.0012
Cl^-	10	0.0441	±0.0013
Ce^{2+}	10	0.0211	±0.0015
Na^+	10	0.0252	±0.0014
Fe^{3+}	10	0.0263	±0.0012
K^+	10	0.0447	±0.0014
Mg^{2+}	10	0.0295	±0.0017
NO_3^-	10	0.0314	±0.0021
SO_4^{2-}	10	0.0145	±0.0016

RSD: relative standard deviation

The precision and validity of Cu_2O@f-MWCNTs/GCE were evaluated for the determination of RHP as strong sedatives and muscle relaxers in prepared real samples of human blood plasma that were provided by healthy volunteers. The findings of amperometric studies at 0.43 V and human Flunitrazepam ELISA kit for determination of RHP in prepared real samples before and after addition of RHP and obtained analytical results using the standard addition method are tabulated in Table 3. As found, there is the good agreement between the outcomes of both analyses. There was acceptable recovery **(**99.40% to 99.60%**)** and low values of RSD (3.22% to 4.87%), which indicated the developed method has been successfully used for RHP determination in biological liquids.

Table 2. The analytical findings of amperometric studies at 0.43 V and human Flunitrazepam ELISA kit for determination of RHP in prepared real samples from human blood plasma.

	Amperometry			*Human Flunitrazepam ELISA kit*		
spiked (µM)	**detected (µM)**	**Recovery (%)**	**RSD (%)**	**detected (µM)**	**Recovery (%)**	**RSD (%)**
0.00	0.00	---	3.87	0.00	---	3.70
5.00	4.97	99.40	4.18	4.96	99.20	4.09
10.00	9.96	99.60	4.87	9.98	99.80	3.88
15.00	14.91	99.40	3.22	15.02	100.13	4.11

4. CONCLUSION

The creation of a nanocomposite of Cu_2O@f-MWCNTs/GCE using the electrodeposition method was presented in this study as a sensitive and specific electrochemical sensor for the measurement of RHP in human blood plasma. According to structural investigations, the Cu_2O nanoparticles were randomly arranged on the surface of the f-MWCNTs, resulting in a high specific surface area and a porous architecture. This indicates that the Cu_2O@f-MWCNTs nanocomposite was successfully electrodeposited on the GCE. The electrochemical studies demonstrated that the Cu_2O@f-MWCNTs/GCE to determine RHP had good selectivity and sensitivity (0.1769 μA/μM), an acceptable detection limit (15 nM), and a wide linearity range (1 to 160 μM). These properties were promoted and were superior to or on par with recent reports of RHP electrochemical sensors. In order to determine RHP in prepared real samples of human blood plasma, the accuracy and validity of Cu_2O@f-MWCNTs/GCE were assessed. The results showed acceptable recovery and low values of RSD, indicating that the developed method has been used successfully to determine RHP as strong sedatives and muscle relaxers in biological liquids.

References

1. C.R. Doyno and C.M. White, *The Journal of Clinical Pharmacology*, 61 (2021) 114.
2. T. Lu, W. Yan, G. Feng, X. Luo, Y. Hu, J. Guo, Z. Yu, Z. Zhao and S. Ding, *Green Chemistry*, 24 (2022) 4778.
3. F. Yu, Z. Zhu, C. Li, W. Li, R. Liang, S. Yu, Z. Xu, F. Song, Q. Ren and Z. Zhang, *Applied Catalysis B: Environmental*, 314 (2022) 121467.
4. S. Sun, H. Liu, Y. Hu, Y. Wang, M. Zhao, Y. Yuan, Y. Han, Y. Jing, J. Cui and X. Ren, *Bioactive Materials*, 20 (2023) 166.
5. T. Yamagishi, A. Akashi, H. Shimizu, T. Ishida, T. Tanabe, K. Sugiyama and Y. Hamabe, *Acute Medicine & Surgery*, 5 (2018) 202.
6. C. Li, T. Jiang, S. Liu and Q. Han, *Aerospace Science and Technology*, 124 (2022) 107513.
7. D. Sun, J. Huo, H. Chen, Z. Dong and R. Ren, *Engineering Failure Analysis*, 131 (2022) 105812.
8. G. Li, H. Yuan, J. Mou, E. Dai, H. Zhang, Z. Li, Y. Zhao, Y. Dai and X. Zhang, *Composites Communications*, 29 (2022)
9. Y. Wang, C. Li, Y. Zhang, M. Yang, B. Li, L. Dong and J. Wang, *International Journal of Precision Engineering and Manufacturing-Green Technology*, 5 (2018) 327.
10. N. Lahane and G. Kaur, *Materials today: proceedings*, 48 (2022) 1240.
11. C.H.-l. Tam, S.I. Kwok, T.W. Lo, S.H.-p. Lam and G.K.-w. Lee, *Frontiers in psychiatry*, 9 (2018) 457.
12. X. Xue, H. Liu, S. Wang, Y. Hu, B. Huang, M. Li, J. Gao, X. Wang and J. Su, *Composites Part B: Engineering*, 237 (2022) 109855.
13. Z. Wang, L. Dai, J. Yao, T. Guo, D. Hrynsphan, S. Tatsiana and J. Chen, *Bioresource Technology*, 327 (2021) 124785.
14. Z. Zhang, P. Ma, R. Ahmed, J. Wang, D. Akin, F. Soto, B.F. Liu, P. Li and U. Demirci, *Advanced Materials*, 34 (2022) 2103646.
15. X. Hu, P. Zhang, D. Wang, J. Jiang, X. Chen, Y. Liu, Z. Zhang, B.Z. Tang and P. Li, *Biosensors and Bioelectronics*, 182 (2021) 113188.

16. D. Shi, Y. Chen, Z. Li, S. Dong, L. Li, M. Hou, H. Liu, S. Zhao, X. Chen and C.P. Wong, *Small Methods*, (2022) 2200329.
17. M.J. Bogusz, R.-D. Maier, K.-D. Krüger and W. Früchtnicht, *Journal of Chromatography B: Biomedical Sciences and Applications*, 713 (1998) 361.
18. L. Gautam, S.D. Sharratt and M.D. Cole, *PloS one*, 9 (2014) e89031.
19. N. Leesakul, S. Pongampai, P. Kanatharana, P. Sudkeaw, Y. Tantirungrotechai and C. Buranachai, *Luminescence*, 28 (2013) 76.
20. S. Pongampai, P. Amornpitoksuk, P. Kanatharana, T. Rujiralai, S. Suwanboon and N. Leesakul, *ScienceAsia*, 37 (2011) 320.
21. P. D'Aloise and H. Chen, *Science & Justice*, 52 (2012) 2.
22. J. Weijers-Everhard, J. Wijker, R. Verrijk, H. Van Rooij and W. Soudijn, *Journal of Chromatography B: Biomedical Sciences and Applications*, 374 (1986) 339.
23. B.M. Asiabar, M.A. Karimi, H. Tavallali and M. Rahimi-Nasrabadi, *Microchemical Journal*, 161 (2021) 105745.
24. E. Sohouli, M. Ghalkhani, M. Rostami, M. Rahimi-Nasrabadi and F. Ahmadi, *Materials Science and Engineering: C*, 117 (2020) 111300.
25. F. Tseliou, P. Pappas, K. Spyrou, J. Hrbac and M.I. Prodromidis, *Biosensors and Bioelectronics*, 132 (2019) 136.
26. E. Garcia-Gutierrez and C. Lledo-Fernandez, *Chemosensors*, 1 (2013) 68.
27. J.P. Smith, J.P. Metters, D.K. Kampouris, C. Lledo-Fernandez, O.B. Sutcliffe and C.E. Banks, *Analyst*, 138 (2013) 6185.
28. M.S. Mohammadnia, E. Naghian, M. Ghalkhani, F. Nosratzehi, K. Adib, M.M. Zahedi, M.R. Nasrabadi and F. Ahmadi, *Journal of Electroanalytical Chemistry*, 880 (2021) 114764.
29. D. Chen, Y. Li, X. Li, X. Hong, X. Fan and T. Savidge, *Chemical Science*, 13 (2022) 8193.
30. Q. Liu, H. Peng and Z.-A. Wang, *Journal of Differential Equations*, 314 (2022) 251.
31. J. Zhang, C. Li, Y. Zhang, M. Yang, D. Jia, G. Liu, Y. Hou, R. Li, N. Zhang and Q. Wu, *Journal of cleaner production*, 193 (2018) 236.
32. A. Ejaz, H. Babar, H.M. Ali, F. Jamil, M.M. Janjua, I.R. Fattah, Z. Said and C. Li, *Sustainable Energy Technologies and Assessments*, 46 (2021) 101199.
33. R. Liu, X. Hu, Y. Cao, H. Pang, W. Hou, Y. Shi, H. Li, X. Yin and H. Zhao, *International Journal of Electrochemical Science*, 17 (2022) 220676.
34. J. xi Ma, Y. Ning, L. Yang, Y. Feng and Y. Liu, *International Journal of Electrochemical Science*, 16 (2021) 211255.
35. M. Guo, T. Wu, G. Zhu, Y. Liu, M. Zhao, Y. Shen, Y. Zhou, L. Chen, X. Guo and Q. Wang, *International Journal of Electrochemical Science*, 17 (2022) 220772.
36. S. Ammara, S. Shamaila, A. Bokhari and A. Sabah, *Journal of Physics and Chemistry of Solids*, 120 (2018) 12.
37. S.K. Singhal, M. Lal, I. Sharma and R.B. Mathur, *Journal of composite materials*, 47 (2013) 613.
38. J. He, P. Xu, R. Zhou, H. Li, H. Zu, J. Zhang, Y. Qin, X. Liu and F. Wang, *Advanced Electronic Materials*, 8 (2022) 2100997.
39. T. Lv, Y. Yao, N. Li and T. Chen, *Angewandte Chemie International Edition*, 55 (2016) 9191.
40. M. Xi, C. He, H. Yang, X. Fu, L. Fu, X. Cheng and J. Guo, *Chinese Chemical Letters*, 33 (2022) 2595.
41. M.M. Ngoma, M. Mathaba and K. Moothi, *Scientific Reports*, 11 (2021) 1.
42. T. Li, M. Sun and S. Wu, *Nanomaterials*, 12 (2022) 784.
43. B. Li, C. Li, Y. Zhang, Y. Wang, D. Jia and M. Yang, *Chinese Journal of Aeronautics*, 29 (2016) 1084.
44. C. Niveditha, A. Nizamudeen, R. Ramanarayanan, M.J. Fatima and S. Swaminathan, *Materials Research Express*, 5 (2018) 035504.

45. T. Li, D. Shang, S. Gao, B. Wang, H. Kong, G. Yang, W. Shu, P. Xu and G. Wei, *Biosensors*, 12 (2022) 314.
46. Z. Dai, A. Yang, X. Bao and R. Yang, *Sensors*, 19 (2019) 2824.
47. C. Lu, Z. Li, L. Ren, N. Su, D. Lu and Z. Liu, *Sensors*, 19 (2019) 2926.
48. J.M. Marioli and T. Kuwana, *Electrochimica Acta*, 37 (1992) 1187.
49. W. Zhang, R. Zhang, M. Shi, L. Ma and Y. Huang, *Electrochimica Acta*, 424 (2022) 140631.
50. Y. Tian, Y. Liu, W.-p. Wang, X. Zhang and W. Peng, *Electrochimica acta*, 156 (2015) 244.
51. T. Gao, Y. Zhang, C. Li, Y. Wang, Q. An, B. Liu, Z. Said and S. Sharma, *Scientific reports*, 11 (2021) 1.
52. L. Hussein, Y. Feng, N. Alonso-Vante, G. Urban and M. Krüger, *Electrochimica acta*, 56 (2011) 7659.
53. W. Yuan, S. Lu and Y. Xiang, *Rsc Advances*, 4 (2014) 46265.
54. W. Zhang, R. Zhang, Y. Tan, Y. Xue, J. Dong, L. Ma, Z. Jiang and Y. Huang, *Composites Science and Technology*, 226 (2022) 109559.
55. P. Viswanathan, K. Wang, J. Li and J.-D. Hong, *Colloids and Surfaces A: Physicochemical and Engineering Aspects*, 598 (2020) 124816.
56. T. Li, W. Yin, S. Gao, Y. Sun, P. Xu, S. Wu, H. Kong, G. Yang and G. Wei, *Nanomaterials*, 12 (2022) 982.
57. J. Liu, T. Li, H. Zhang, W. Zhao, L. Qu, S. Chen and S. Wu, *Materials Today Bio*, 14 (2022) 100243.
58. M. Yang, C. Li, Z. Said, Y. Zhang, R. Li, S. Debnath, H.M. Ali, T. Gao and Y. Long, *Journal of Manufacturing Processes*, 71 (2021) 501.